ORIGINAL ARTICLE

Estimating wheat evapotranspiration through remote sensing utilizing GeeSEBAL and comparing with lysimetric data

Neda Baboli[1] · Houshang Ghamarnia[2] · Maryam Hafezparast Mavaddat[2]

Abstract

Accurate estimation of ET is vital for water resource management. In recent decades, researchers have focused on utilizing satellite imagery for this purpose. The use of RS data has enabled the development of new models that provide detailed spatial assessments. GeeSEBAL, an automated ET estimation tool, employs the SEBAL algorithm via GEE. The current version of GeeSEBAL utilizes Landsat images and ERA5 global reanalysis data to produce time series estimates. Landsat 8 images were processed into a 16-day time series spanning 2013–2022, specifically during the wheat growing season. To validate the GeeSEBAL model for 2013–2014, results were compared against lysimeter data. Subsequently, ET was calculated for the years 2015–2022. The evaluation of GeeSEBAL against lysimetric data, by metrics such as R^2, RMSE, MAE, NSE, and NRMSE, yielded values of 0.94, 0.98, 0.07, 0.86, and 0.62, respectively. Those findings underscore the importance of GeeSEBAL for estimating wheat ET in regions with limited data availability.

Keywords ET · SEBAL algorithm · GeeSEBAL · GEE environment · ERA5 weather data

Abbreviations

API	Application programming interface
EC	Eddy covariance
ET	Evapotranspiration
DEM	Digital elevation model
GEE	Google Earth Engine
GeeSEBAL	Google Earth Engine Surface Energy Balance Algorithm
GIS	Geographic information system
GT	Greenwich time
MAE	Mean absolute error
NSE	Nash–Sutcliffe efficiency
NRMSE	Normalized root mean square error
RS	Remote sensing
RMSE	Root mean squared error
R^2	Determination coefficient

✉ Maryam Hafezparast Mavaddat
maryam.hafezparast@gmail.com; m.hafezparast@razi.ac.ir

Neda Baboli
neda3701@gmail.com

Houshang Ghamarnia
hghamarnia@razi.ac.ir; hghamarnia@yahoo.co.uk

[1] Irrigation and drainage Engineering, Department of Water Engineering, Campus of Agriculture and Natural Resources, Razi university, Kermanshah, Iran

[2] Department of Water Engineering, Campus of Agriculture and Natural Resources, Razi university, Kermanshah, Iran

Introduction

One of the key economic and social challenges in developing nations, particularly those in barren and semiarid regions, is water shortage (Wu et al. 2018). Iran, with much of its land in arid and semiarid zones, relies heavily on water and irrigation for agriculture (Karandish and Hoekstra 2017). As the global population is projected to reach 7.8 billion by 2025, there will be heightened pressure on food security in developing nations, home to over 80 percent of this increase. Consequently, these countries will confront water scarcity in meeting agricultural, industrial, and urban demands (Nazari et al. 2013). Thus, accurate water demand forecasting is crucial for agriculture (Gonçalves et al. 2022). ET estimation is a method that enhances water management, leading to improved water efficiency (Venancio 2019).

Numerous methods have been developed and studied using meteorological data to calculate ET in various climatic and geographic conditions. These methods range from simple empirical relationships to those with a complex physical basis. Most rely on point-to-point measurements, limiting their applicability to local areas and making them

unsuitable for large basins due to the dynamic and regional nature of ET (Volk et al. 2023). Remote sensing technology and geographic information systems are commonly used for estimating ET, especially in extensive areas (Yao 2019). By utilizing satellite imagery, which contains valuable information for estimating actual ET, researchers have developed methods to reduce reliance on ground data. Satellite images provide data on different surface properties across various bands of visible, thermal, and infrared spectra, enabling the estimation of real ET (Zhou et al. 2014).

RS is the sole technology capable of extracting parameters like surface temperature, albedo coefficient, and plant index in an efficient and environmentally friendly manner, while also being cost-effective (Campos et al. 2018). GEE stands out as a top-notch web-based RS system that has greatly simplified numerous satellite image processing tasks in recent years (Gorelick et al. 2017). The primary objective in estimating ET is to boost agricultural output with reduced water usage, thereby decreasing the agricultural water footprint and reallocating water to other purposes, particularly environmental needs. Currently, the agricultural sector, through global research initiatives like the Global Research on Water and Food Challenges led by the International Agricultural Research Advisory Group, aims to utilize excess water across various economic sectors to not only enhance productivity but also improve community livelihoods and environmental conditions. Consequently, these programs strive to enhance agricultural production per unit of water, starting from plant level and extending to irrigation systems and watersheds.

Recent years have seen valuable research on estimating ET under changing climate conditions worldwide. Gonçalves et al. (2022) examined RS ET determination using GeeSEBAL for sugarcane irrigation management in Brazil. Landsat 8 (OLI) and Landsat 7 (ETM+) satellite images were employed in the study, revealing energy balance components computed by GeeSEBAL to be acceptable with $R^2 = 0.97$. Kayser et al. (2022) explored GeeSEBAL's automatic calibration uncertainty for estimating ET in subtropical humid climates, validating ET estimates with air circulation covariance measurements. Processing 132 cloudless Landsat images yielded an RMSE value of 0.91 mm/day and R^2 of 0.82. Sun et al. (2022) assessed changes in water use efficiency and its correlation with land use changes using three different data inputs in China's Yellow River. The paper proposed a framework for real ET processing and WUE calculation through the maximum entropy generation method and GEE environment. By applying this framework and utilizing the three data inputs in GEE, ET and real WUE results were computed from 2001 to 2020. The study demonstrated that this system, combined with the maximum entropy production method, presents new opportunities for enhancing water resources management.

This study aimed to introduce and evaluate new methods for estimating ET using satellite data in the Kermanshah plain lands. The research employed Google Earth Reference ET Engine products and the SEBAL energy balance algorithm to calculate actual ET via the GeeSEBAL model on GEE. To evaluate global and national initiatives in the field of ET, OpenET and FAO Wapor were utilized. Landsat satellite images at a 30 × 30-meter resolution from 2013 to 2022, corresponding to the wheat cultivation period in Kermanshah plain, were used to estimate wheat plant ET. The ET time series was generated by utilizing advanced weather data reanalysis from ERA5. The expected outcome of this study is an improvement in water resource management through sustainable methods, offering managers precise information derived from ET data access.

Materials and methods

The study area

Kermanshah province, situated in the western part of the country, relies heavily on agriculture for its economy. The Kermanshah plain, spanning 28797 hectares, is positioned between 46°45′ and 47°5′ east longitude and 34°23′ to 34°35′ north latitude (Fig. 1). Every year almost 109,000 hectares of Kermanshah farms are cultivated with wheat. The average elevation of the plain is 1330 meters above sea level, with an average annual temperature of 14.1 degrees Celsius and a total rainfall of 458 mm. Kermanshah is divided into 14 counties and shares borders with Kurdistan province to the north, Lorestan and Ilam provinces to the south, Hamedan province to the east, and Iraq to the west, with over 330 km of common border. The region experiences most of its precipitation from humid Mediterranean fronts, resulting in rain and hail during autumn and spring, and snow during winter. Wheat is the primary agricultural product in the region, covering the largest portion of agricultural land.

Lysimeter specification

Studies of wheat ET in 2013 and 2014 were carried out at the Research Farm of Water Resources Engineering Department located on the campus of Faculty of Agriculture and Natural Resources of Razi University of Kermanshah, which has a longitude of 47° 9" east and latitude of 34° 21" north and is located at an altitude of 1319m above sea level. During the study, meteorological data were collected daily from a fully automated meteorological station located 50 m from the lysimetric station site.

Six drainable lysimeters with diameter of 1.20 and depth of 1.20 m were used for this research and wheat was planted on them. The soil texture used in lysimeters was silty clay and its moisture content in the range of soil agronomic capacity was 24% by weight and its specific bulk density was 1.3 g/cm³.
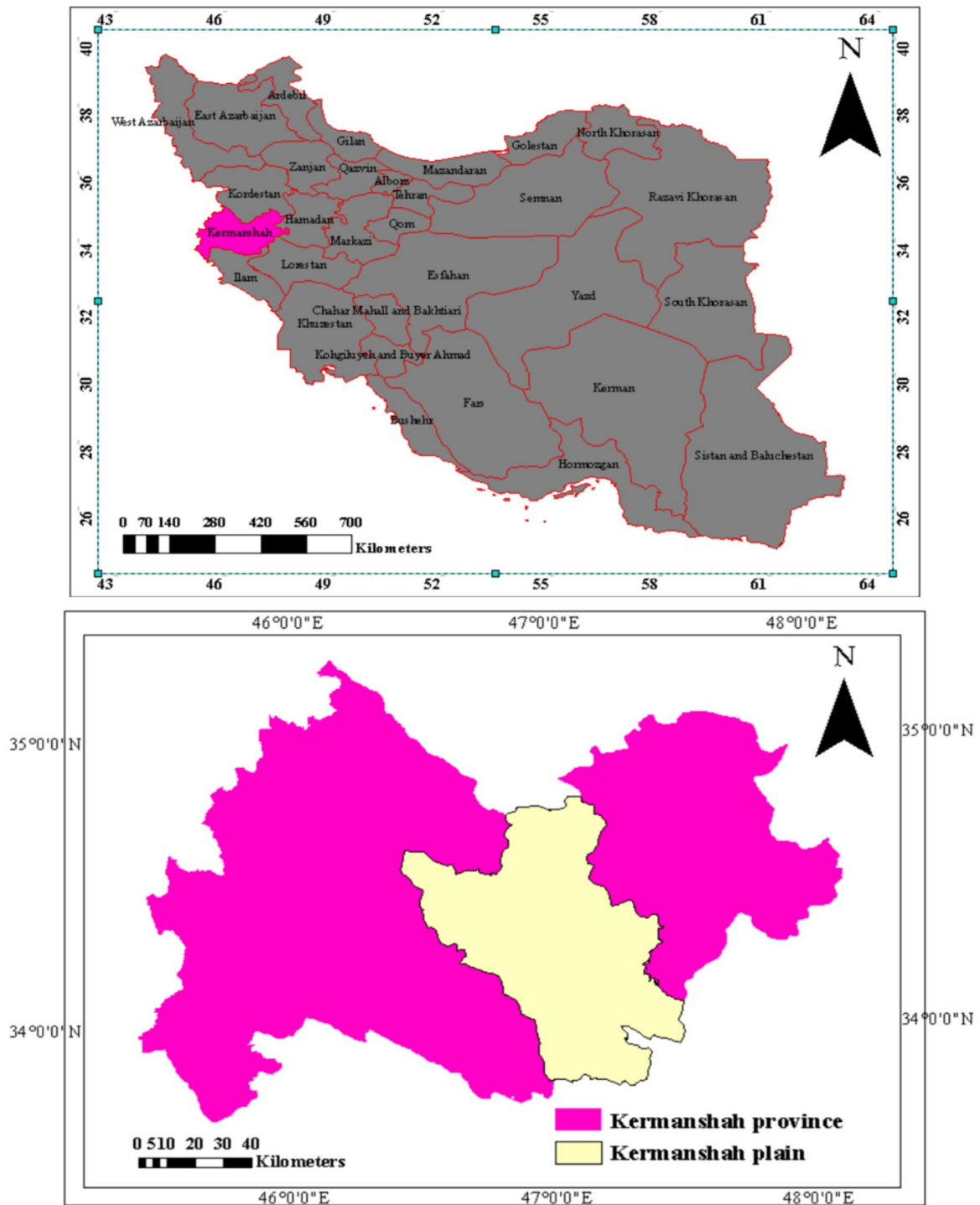
Fig. 1 Location of the study area in Iran and Kermanshah province

Sampling was started with the beginning of the growing season. In each record, the values of irrigation depth, rainfall, drainage, and changes in soil moisture reserve were recorded and using water balance equation, the actual ET and ET of wheat plants were determined.

The irrigation cycle was selected in a way that the lowest stress was applied to the plant. To measure ET by drained lysimeter for a given period of time, the water balance of the soil was used as Eq. 1.

$$ETc = I + P - D \pm \Delta S \qquad (1)$$

where ETc = wheat ET (mm); I= irrigation depth (mm); P= precipitation (mm); D= depth of drainage water (mm); ΔS = changes in soil moisture in the given period (mm).

During irrigation, the value of moisture content in soil profile was measured using TDR equipment and installed the corresponding sensors at depths of 10, 30, 60, and 80 cm inside of the drainable lysimeters. Excess water extracted from lysimeters that was drained using underground pipes into tanks in the underground access chamber adjacent to the lysimeters was measured by a calibration container (Fig. 2).

Satellite images used

The satellite images used in the study include Landsat 8 images taken at 16-day intervals during the wheat growing season from 2013 to 2022, ensuring that there are no clouds covering the area. The specific date and time of the satellite imaging are detailed in Table 1. Kermanshah synoptic station served as the reference station (Fig. 3). Essential meteorological parameters for the study encompass solar radiation, relative humidity, wind speed, and temperature on satellite transit days. GeeSEBAL, a novel tool for automated ET estimation, employs SEBAL via GEE. The study integrated GIS and GEE.
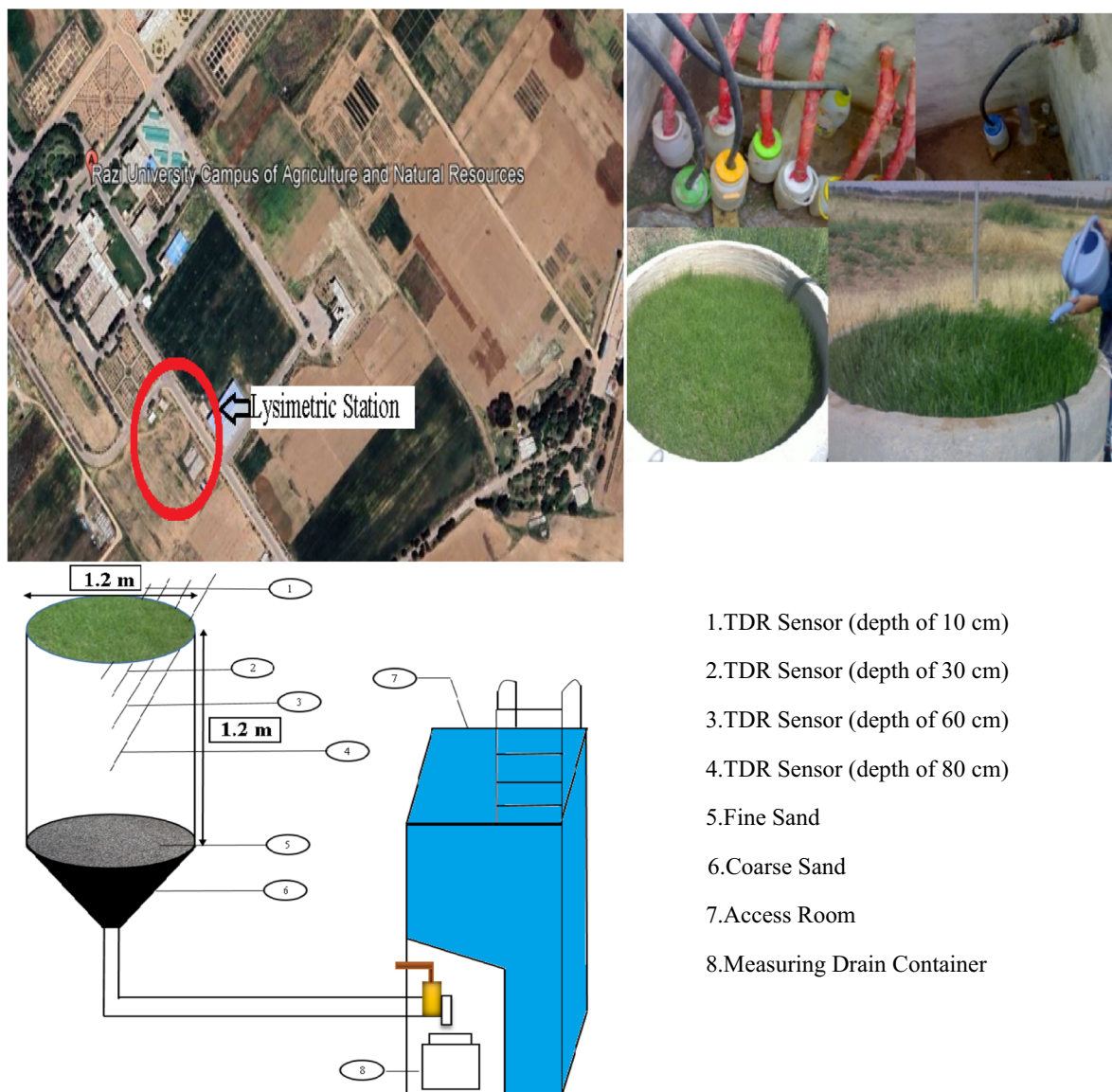
1. TDR Sensor (depth of 10 cm)

2. TDR Sensor (depth of 30 cm)

3. TDR Sensor (depth of 60 cm)

4. TDR Sensor (depth of 80 cm)

5. Fine Sand

6. Coarse Sand

7. Access Room

8. Measuring Drain Container

Fig. 2 Location of drainage lysimeters in the agricultural campus of Razi University to calculate the ET of wheat plants

Table 1 Satellite imagery used in the research

Date of image capture	Time of image capture (GT)	Date of image capture	Time of image capture (GT)	Date of image capture	Time of image capture (GT)
2013/06/01	07:29:05	2016/06/09	07:26:43	2020/04/17	07:26:37
2013/06/17	07:28:59	2016/06/25	07:26:50	2020/05/19	07:26:28
2014/04/01	07:27:15	2017/05/11	07:26:25	2020/06/04	07:26:34
2014/05/03	07:26:44	2017/05/27	07:26:36	2020/06/20	07:26:44
2014/06/20	07:26:45	2017/06/12	07:26:43	2021/04/04	07:26:48
2015/04/04	07:26:25	2017/06/28	07:26:48	2021/06/07	07:26:50
2014/04/20	07:26:24	2018/06/15	07:25:56	2021/06/23	07:26:55
2015/05/06	07:26:10	2019/04/15	07:26:30	2022/04/23	07:26:50
2015/06/07	07:26:15	2019/05/17	07:26:38	2022/05/09	07:26:55
2015/06/23	07:26:21	2019/06/02	07:26:46	2022/06/10	07:25:09
2016/04/22	07:26:34	2019/06/18	07:26:53	2022/06/26	07:27:16

Fig. 3 Location of the study area, synoptic and lysimetric stations in GEE

SEBAL algorithm

The immediate calculation of transpiration evaporation (λET) for satellite transit time is determined by the net radiation flux (Rn), sensible heat flux (G), and soil heat flux (H) values per pixel as per the equation by Jiang et al. (2015).

$$\lambda\text{ET} = \text{Rn} - G - H \tag{2}$$

Net radiation (Rn)

The net radiation flux at the Earth's surface is calculated using the balance equation of the diffusion flux from the atmosphere to the surface. The amount of net radiation on the Earth's surface is determined by the following equation.

$$\text{Rn} = (1 - \alpha)\text{Rs} \downarrow + \text{RL} \downarrow - \text{RL} \uparrow - (1 - \varepsilon_0)\text{RL} \downarrow \tag{3}$$

where α Albedo, Rs↓ incoming shortwave radiation (0.3–μm) (W/m2), RL↓ incoming longwave radiation (3–100 μm) (W/m^2), RL↑ longwave output (W/m^2), ε_0 surface emissivities.

Calculation of albedo surface (α)

Albedo represents the ratio of reflected solar radiation to the total solar radiation received on Earth's surface. This value is influenced by the characteristics, composition, and intensity of solar radiation. The surface albedo for individual pixels in satellite imagery is determined using Eq. 4 (Silva et al. 2018).

$$\alpha = \frac{\alpha_{\text{toa}} - \alpha_{\text{path - radiance}}}{\tau_b^2} \tag{4}$$

In the above equation, τ_b is the atmospheric transmission coefficient and α_{toa} is the albedo in suitable atmospheric conditions, which is calculated from Eq. 5. Also, $\alpha_{\text{path−radiance}}$ is the amount of deviant radiation albedo, the average solar radiation in all bands that are reflected to the sensor through the atmosphere before reaching the earth, is a value between 0.025 and 0.04.

$$\alpha_{\text{toa}} = \sum \left(W_\lambda \times \rho_\lambda \right) \tag{5}$$

In Eq. 4, ρ_λ is the reflectivity rate for band λ and ρ_λ is the weight coefficient for λ, which is calculated as Eq 6.

$$W_\lambda = \frac{\text{ESUN}_\lambda}{\sum \text{ESUN}_\lambda} \tag{6}$$

According to the above relationship, ESUN_λ is the average exo-atmospheric brightness for the λ band, whose value is different for each band and a constant value for each Satellite image sensor (Richter et al. 2009). The coefficients of each reflective band of Landsat 8 images for albedo calculation are shown in Table 2.

Normalized difference vegetation index (NDVI)

Vegetation indicators were enhanced with the introduction of the initial satellites designed for monitoring and assessing vegetation cover (Huete and Glenn 2011). This index relies on vegetation quantity and health. NDVI is computed using infrared and near-infrared bands satellite data.

$$\text{NDVI} = \frac{\rho_{\text{NIR}} - \rho_R}{\rho_{\text{NIR}} + \rho_R} \tag{7}$$

In which ρ_{NIR} is the reflectivity recorded in the near-infrared band and ρ_R is the reflectivity recorded in the infrared band. In different sensors, the bands of infrared and near-infrared wavelengths are different. In Table 3, the infrared and near-infrared bands in the OLI sensor are shown.

Soil adjusted vegetation index (SAVI)

The SAVI index is an indicator to eliminate the effects of background soil on the NDVI index.

$$\text{SAVI} = \frac{\rho_{\text{NIR}} - \rho_R}{\rho_{\text{NIR}} + \rho_R + L}(1 + L) \tag{8}$$

In which L is a factor for eliminating the effects of vegetation that ranges from zero for dense vegetation to 1 for low density.

Leaf area index (LAI)

LAI is the ratio of the total area of the plant leaves to its canopy. Different relationships have been developed to obtain leaf area index, one of these methods is as follows:

$$\text{LAI} = \frac{-\ln\left(\frac{0/69 - \text{SAVI}}{0/59}\right)}{0/91} \tag{9}$$

Calculation of incoming short-wavelength radiation ($R_s\downarrow$)

Incoming short-wavelength solar radiation is the sunlight that reaches Earth's surface directly or diffusely under clear sky conditions. This value is influenced by atmospheric factors, time, and location, and can be determined using relationships (10) to (12).

$$R_S \downarrow = G_{\text{sc}} \times \text{COS}\theta \times \text{dr} \times \tau_{\text{sw}} \tag{10}$$

$$\text{dr} = 1 + 0/0033 \times \text{COS}((\text{DOY} \times 2\pi)/365) \tag{11}$$

$$\tau_{\text{sw}} = 0/75 + 2 \times 10 - 5 \times Z \tag{12}$$

Table 3 Infrared and near-infrared bands in OLI sensor

Image sensor	Infrared	Near infrared
OLI	Band 4	Band 5

Table 2 Coefficients of reflective bands of Landsat 8 images

Band	Band 1	Band 2	Band 3	Band 4	Band 5	Band 6	Band 7	Fixed
Landsat8	0.356	0	0.130	0.373	0.085	0.072	0.072	− 0.0018

The solar constant GSC is 1367 (Wm^{-2}). The angle θ is 90°-β, where β represents the altitude angle of the Sun. The term dr squared inversely represents the relative distance of the Earth to the Sun, which is derivable from the Day of Year (DOY) and τ_sw, the atmospheric permittivity. The latter is determined using the Z zone average height, which is better calculated using the DEM instead of the area's average height for more precise outcomes. RS↓ can vary between 200 and 1000 depending on the specific time and location of the image.

Calculation of incoming longwave radiation ($R_L\downarrow$)

The incoming longwave radiation is the thermal flux entering the atmosphere to the surface of the earth in terms of W/m^2 calculated by the Stephen–Boltzmann equation as (13).

$$R_L \downarrow = \varepsilon_a \sigma T_a^4 \tag{13}$$

In relation to (13), ε_a is the atmospheric emission coefficient, σ is the Stephen–Boltzmann constant, and T_a is the near-surface air temperature in degrees Kelvin. In this context, the cold pixel temperature can be considered as the air temperature near the surface. To calculate the emission coefficient, the following empirical relation can be utilized.

$$\varepsilon_a = 0/85 \times \left(-\ln \tau_{sw}\right)^{0/09} \tag{14}$$

In relation to (14), τsw is the atmospheric transit coefficient. The incoming long wavelength radiation has values ranging from 200 to 600 (Wm^{-2}).

Calculation of outgoing longwave radiation ($R_L\uparrow$)

The outgoing longwave radiation is calculated according to Stephen–Boltzmann's law and using the (15) relation.

$$R_L \uparrow = \varepsilon_0 \times \sigma \times T_S^4 \tag{15}$$

In relation to (15), $R_L\uparrow$ longwave radiation, ε_0 power that represents thermal radiation behavior in the range of 6–14 microns and T_S (Kelvin) surface temperature.

Earth surface temperature (T_s)

Surface temperature is one of the main parameters for calculating SEBAL algorithm.

Surface temperature of Landsat Satellite 8

In Landsat 8, thermal bands 10 or 11 are used to calculate surface temperature. In this study, the following relationship is used to estimate the surface temperature.

$$T_S = \frac{K2}{\ln\left(\frac{\varepsilon_{NB}K1}{RC} + 1\right)} \tag{16}$$

In the above relationship, RC is a surface corrected thermal radiance for bands 10 or 11 Landsat 8, values of $K1$ and $K2$ are constant values equal to 774.89 and 1321.08, respectively, and εNB emission coefficient in low bands of thermal width which can be calculated with ε_0 according to the below table.

Surface emission (εNB)

Surface emission is the ratio of heat energy radiated by the surface to the heat energy radiated by the black body at the same temperature. The surface emissivity for the earth's surface coverage, established through empirical relations, is presented in Table 4 (Allen et al. 2005).

Hot and cold pixels

The SEBAL method uses two square pixels of indicators to determine the constant boundary conditions in the energy balance equation. One of these pixels, called the cold pixel, is from a well-watered and well-watered area, the ground surface temperature in this pixel is close to the air temperature and the evaporation and sweating equivalent to ET is referenced. The second pixel, called the warm pixel, is dry and vegetation-free agricultural land where ET is considered zero.

Soil heat flux (G)

Soil heat flux is the amount of heat transfer within the soil and vegetation due to molecular conductivity. The following equation can be used to calculate it (de Lima et al. 2021).

$$\frac{G}{Rn} = \frac{T_s}{\alpha} \times \left(0/0032 \times \alpha + 0/0062 \times \alpha^2\right) \times \left(1 - 0/978 \times NDVI^4\right) \tag{17}$$

In this regard, T_s is surface temperature, surface albedo α, NDVI vegetation index, and solar net radiation Rn. The above relationship has acceptable performance in agricultural lands.

Table 4 Surface emissions based on land cover

NDVI ≥ 0	LAI < 3	$\varepsilon_{NB} = 0/97 + 0/0033 \times LAI$
		$\varepsilon_0 = 0/95 + 0/01 \times LAI$
	LAI ≥ 3	$\varepsilon_{NB} = 0/98$
		$\varepsilon_0 = 0/98$
NDVI < 0	For water (α<0/47)	$\varepsilon_{NB} = 0/99$
	For snow ($\alpha\geq$0/47)	$\varepsilon_0 = 0/985$

In SEBAL, the ratio of G/R_n for clear, deep water, and snow is equal to 0.5.

This ratio is estimated using the values of net radiation flux, heat flux, and soil heat flux obtained at the time of imaging (Ferreira et al. 2013).

$$\Delta_{ins} = \frac{R_n - G - H}{R_n - G} \tag{18}$$

Heat flux (H)

The last parameter in the energy balance equation is the H (the permeable heat flux). Thermal heat flux is the amount of heat loss to air by convection and molecular conductivity due to the difference in temperature. The most important and difficult part of SEBAL's algorithm is to calculate the heat flux based on heat transfer and can be calculated through the following equation (Wang et al. 2020).

$$H = \frac{\rho \times Cp \times d_T}{r_{ah}} \tag{19}$$

In the above relationship, ρ represents the air density (Kg/m^3), Cp is the specific heat of air (1004J/kg/k), dT denotes the temperature difference T1-T2 at heights Z1-Z2 in Kelvin, and rah stands for the aerodynamic resistance for heat transfer (m/s). The challenge in computation arises from the presence of two unknowns, r_{ah} and d_T, in Eq 19, making it a complex problem to solve. To simplify the calculations and address this issue, the method involves utilizing two hot and cold pixels as discussed earlier to derive dependable estimates for H.

To account for the impact of buoyancy resulting from surface heating, SEBAL incorporates the Monin–Obukhov theory through an iterative procedure. When computing the sensible heat flux, it is crucial to account for atmospheric stability conditions, particularly under dry circumstances. The atmosphere can exist in three stable states: unstable, neutral, and stable. The stability or instability of the air is determined by the Monin–Obukhov length, where an atmosphere is considered unstable if $L<0$, neutral if $L=0$, and stable if $L>0$. The Monin–Obukhov length is calculated using the following equation (Sun et al. 2011).

$$L = \frac{\rho Cp U*^3 \ T_s}{Kg H} \tag{20}$$

In SEBAL algorithm, we first obtain the initial values of U_* and rah in the meteorological station by assuming neutral atmospheric conditions:

$$r_{ah} = \frac{\ln\left(\frac{Z_2}{Z_1}\right)}{U_* \times K} \tag{21}$$

$$U_* = \frac{KU_x}{\ln\frac{Z_x}{Z_{om}}} \tag{22}$$

$$Z_{om} = 0/12 \times h \tag{23}$$

$$U_{200} = U_* \frac{\ln\left(\frac{200}{Z_{om}}\right)}{K} \tag{24}$$

In the relationship between $Z1$ and $Z2$, elevations above displacement are zero when $Z1$ equals vegetation height and $Z2$ is slightly higher. The SEBAL algorithm uses 0.1 m and 2 m for these values. K is the Van Carmen constant at 0.41. U$_*$ represents frictional velocity indicating turbulence fluctuations in air (m/s), Z_{om} is momentum roughness, Ux is wind speed at Zx height, and H is average vegetation height in meters. Initially, Zom is calculated by averaging vegetation height near the weather station. Then, the target altitude with average wind speed at that level is determined, yielding $U*$ for the weather station using the mentioned formulas. Subsequently, rah for the weather station is computed. With $U*$ and rah known, U200 for the weather station is derived, followed by calculating rah for the entire satellite image. To find the total image r_{ah}, Z_{om} for the whole satellite image is necessary. If a land use map is available, Z_{om} per pixel can be obtained from a provided Table 5.

For agricultural areas and if there is no map available, the value of Z_{om} or as a function of the leaf area index is calculated:

$$Z_{om} = 0/018LAI \tag{25}$$

Or by using albedo and NDVI from the following relationship.

$$Z_{om} = \exp\left[a\left(\frac{\text{NDVI}}{\alpha}\right) + b\right] \tag{26}$$

The coefficients of a and b are based on the sampling of the area can be estimated.

Table 5 Z_{om} values for types of ground surfaces

Land type	Water	City	Jungle	Meadow	Desert or vegetation	Snow
Z_{om}	0.0005	0.2	0.5	0.02	0.1	0.005

In the next step, we need to get the dT value for the points of the image so that we can reach the final goal of calculating the heat flux. In the previous steps, we selected hot and cold pixels and took their main information. In cold pixels, it is assumed that all the energy is spent on evapotranspiration. On the other hand, in the warm pixel that is without vegetation or water, we assume that the rate of ET is zero. The choice of these two pixels requires skill and practice, and the quality of ET calculations depends on the precise selection of these two pixels. By specifying hot and cold pixels, the difference in air temperature and aerodynamic temperature can also be estimated. Thus, between the surface temperature (T_s) of two hot and cold pixels and the difference in temperature dT_{cold} and dT_{hot}, they establish a regression relationship ($dT=b+aT_s$) and by finding the regression coefficients (a), (b) and specifying the total dT, they estimate the value of H with r_{ah}. dT for two hot and cold pixels is obtained through the following relationships.

$$dT_{cold} = \frac{H_{cold} \times r_{ah\text{-}cold}}{\rho \times C_p} \tag{27}$$

$$dT_{hot} = \frac{H_{hot} \times r_{ah\text{-}hot}}{\rho \times C_p} \tag{28}$$

In hot and cold pixels, the heat flux is obtained from the following relationships.

$$H_{hot} = Rn - G \tag{29}$$

$$H_{cold} = Rn - G - K\lambda ET_{ref} \tag{30}$$

In which λET_{ref} is equal to hourly reference ET and is estimated through the FAO Penman–Monteith relation. The K-factor per cold pixel of the plant creates a high sensitivity in the SEBAL model, and its determination requires the coverage information in the cold pixel coordinates. On the other hand, the air temperature for pixels is calculated from the following Eq 31.

$$T_{air} = T_s - d_T \tag{31}$$

By calculating the air temperature for each pixel, the air density can be corrected and the initial H value for each pixel can be calculated by inserting into the equation. By specifying the initial perceptible flux, it is necessary to calculate the length of Monin–Obukhov described earlier. Then, we get the modified values U and r_{ah} using the following relations.

$$U_* = \frac{U_{200}K}{\ln\left(\frac{200}{Z_{om}}\right) - \emptyset_m(200m)} \tag{32}$$

$$r_{ah} = \frac{\ln\left(\frac{z_2}{z_1}\right) - \emptyset_{hz_2} + \emptyset_{hz_1}}{KU_*} \tag{33}$$

In these relationships, $\emptyset m$ (200 m), stability correction for momentum transfer at 200 m and $\emptyset h$ (z2) and $\emptyset h$ (z1), respectively, are stability corrections for heat transfer at 2 and 0.1 m, respectively.

If $L<0$:

$$\emptyset_m(200m) = 2\ln\left(\frac{1 + X_{200m}}{2}\right) + \ln\left(\frac{1 + X^2(200m)}{2}\right)$$
$$- 2ARCTAN(X_{200m}) + 0/5\pi \tag{34}$$

$$\emptyset_h(2m) = 2\ln\left(\frac{1 + X^2(2m)}{2}\right) \tag{35}$$

$$\emptyset_h(0/1m) = 2\ln\left(\frac{1 + X^2(0/1m)}{2}\right) \tag{36}$$

If $L>0$:

$$\emptyset_m(200m) = -5\left(\frac{2}{L}\right) \tag{37}$$

$$\emptyset_h(2m) = -5\left(\frac{2}{L}\right) \tag{38}$$

$$\emptyset_h(200m) = -5\left(\frac{0/1}{L}\right) \tag{39}$$

If $L = 0$:

$$\emptyset_m, \emptyset_h = 0 \tag{40}$$

In these relations, the values x200, x2, and x 0/1 are obtained from the following relations:

$$X(200m) = \left(1 - 16\frac{200}{L}\right)^{0/25} \tag{41}$$

$$X(0/1m) = \left(1 - 16\frac{0/1}{L}\right)^{0/25} \tag{42}$$

Calculation of ET

Finally, to calculate ET in mm/day, we use the following formula:

$$ET_{inst} = 3600\frac{\lambda ET}{\lambda} \tag{43}$$

In this formula, λ is the latent heat of vaporization, which is 2450 J/g. If we want to calculate the amount of ET in mm/day, we use the following equation:

$$ET_r F = \frac{ET_{inst}}{ET_r} \tag{44}$$

Reference ET is calculated using available meteorological data, using FAO Penman–Monteith and ETinst, calculated hourly ET in the previous step. The amount of daily ET is obtained from the following relationship:

$$ET_{24} = ET_r 24 \times ET_r F \tag{45}$$

$ET_r 24$ is the reference ET throughout the day. Finally, ET maps can be prepared and stored using the above relationships (Silva et al. 2018).

GeeSEBAL

The GeeSEBAL algorithm was created within the GEE using JavaScript and implements the SEBAL algorithm. The emergence of the GEE has significantly transformed satellite image processing, accelerating data processing and calculation, thereby enhancing the efficiency of RS in earth sciences. Improved computational speed, automation, and

development of user-friendly algorithms are key attributes of this system. This system enables rapid access to large satellite image datasets without the need for extensive downloads or complex processes in RS software (Gorelick et al. 2017). This study utilized the ERA5 reanalysis dataset for meteorological inputs (Munoz-Sabater et al. 2021). Figure 4 illustrates the calculation stages of wheat ET using the GeeSEBAL model.

Daily real ET (mm d^{-1}) estimated by SEBAL is calculated using the following equation (Bastiaanssen 2000).

$$ET = 0.035 \times \left(\frac{LE}{Rn - G}\right)[(1 - \alpha)Rs - 110\tau 24h] \tag{46}$$

where LE, latent heat flux (W m^{-2}); rn, Net radiation (W m^{-2}); G, soil heat flux (W m^{-2}); α, surface albedo; Rs, daily global solar radiation (W m^{-2}); $\tau 24h$, the average daily atmospheric transmittance.

In this algorithm, a linear equation (dT= $a+b$Tsup) is assumed between air temperature (dT) and surface temperature. Here, 'a' and 'b' represent calibration coefficients. In the cold pixel, H=0, and in the warm pixel, LE=0 (Oliveira et al. 2014). The SEBAL algorithm, developed in GEE, is implemented using JavaScript exclusively for Landsat8 images. GEE provides free access with a vast and expanding user base, access to all Landsat images, direct management of
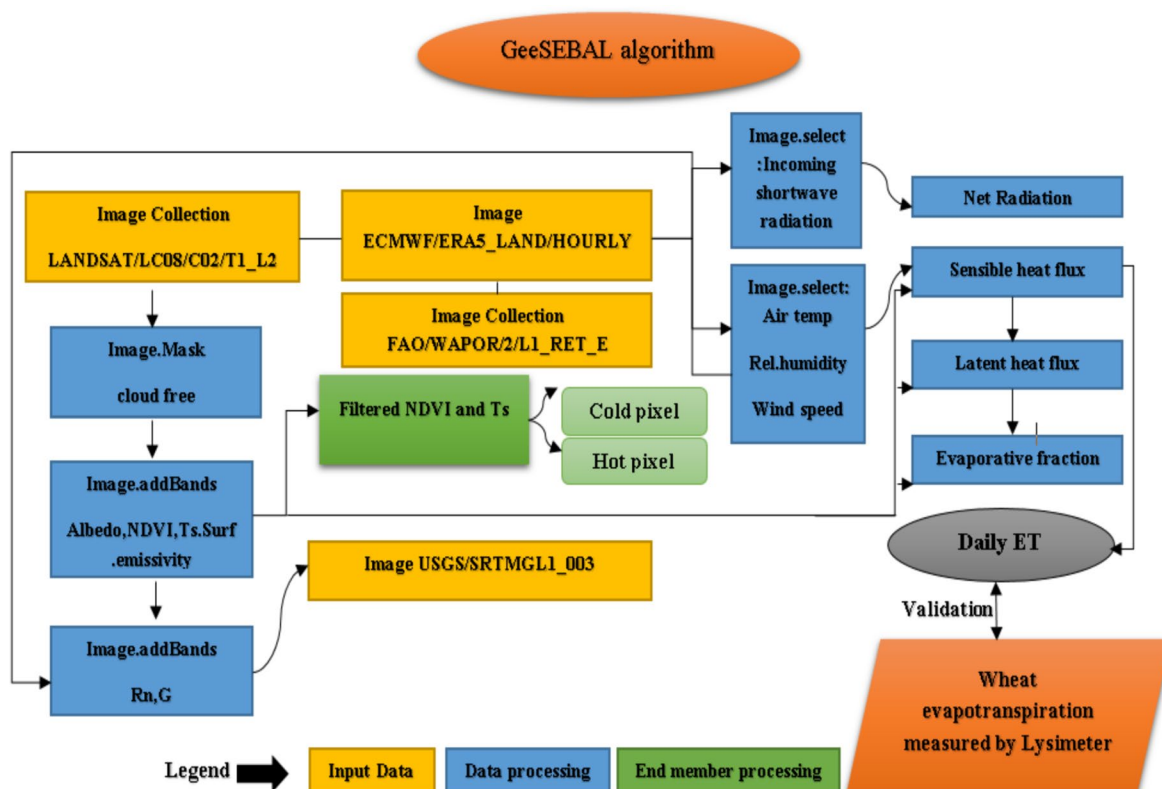

Fig. 4 Steps to calculate ET using GeeSEBAL algorithm.

time series stacks, and ease of parallel processing to quicken calculations. GEE is an integrated environment designed for petabyte-scale scientific analysis and visualization of spatial datasets. The system offers a vast data list analyzed by thousands of computers (Xiong et al. 2017). Users can request new catalogs to be added to the public catalog, upload their data via the REST interface using command-line or browser-based tools, and share with other users or groups as desired. Users can access public data as well as their private data using the operator library provided by the API in GEE and analyze them. These operators are part of a large parallel processing system that automatically distributes calculations and ensures high throughput (Patel et al. 2015).

Model validation

In 2013 and 2014, the GeeSEBAL model's accuracy was assessed by comparing the results with lysimeter data using metrics such as R^2, RMSE, MAE, NSE, and NRMSE that are presented in Table 6. RMSE values indicate errors in statistical methods. Lower RMSE values signify higher model accuracy, with zero indicating perfect estimation. Absolute error ranges from zero to infinity, always positive; closer to zero implies better performance. NSE ranges from -∞ to 1, with 0 to 1 considered acceptable and 1 being optimal. Correlation coefficient values range from 0 to 1; closer to 1 indicates better performance. Variable estimate accuracy is classified into four categories based on NRMSE values: NRMSE<0.2, 0.2≤NRMSE<0.3, 0.3≤NRMSE<0.5, and NRMSE≥0.5 (Li et al. 2013).

In which Si is the estimated value, $\overline{S}$ is the mean of the estimated value, Oi is the observed value, $\overline{O}$ is the mean of the observed value, and N is the number of data.

Results and discussion

The study aimed to compare GeeSEBAL model results for estimating ET of wheat plant with data from ground (lysimeter). GEE coding was used to calculate actual ET in the study area. The basin shapefile has been uploaded to the GEE environment, and the GeeSEBAL code results, including a histogram, ET colorful map, and ET values, are displayed in Fig. 5.

Based on data from a 10-year research period, the satellite passed over the study area a total of 33 times without clouds between 2013 and 2022. Reference ET in this study was computed using established products in GEE, utilizing the FAO Penman–Monteith relationship. In order to validate the results of GeeSEBAL algorithm, 2013 and 2014 lysimetry results were selected and finally the ET values were calculated for other years as well. The average ET values derived from the GeeSEBAL algorithm for each satellite image captured for 2013 and 2014 are detailed in Table 7.

Considering that the goal was to compare the model with the lysimeter, the years 2013 and 2014 were chosen to determine the NDVI and LST values. The subsequent images display the minimum and maximum values of NDVI and LST recorded in the region on various dates. These visual representations allow for the adjustment of hot and cold pixel values in the region (Fig. 6).

In Figs. 7 and 8, dated 01/06/2013 and 20/06/2014, the ET in Kermanshah plain, as per the GeeSEBAL algorithm results, shows an increase. This rise is attributed to the growth in crop vegetation, air temperature, and subsequently ET in these regions. Analysis of the maps indicates that well-irrigated areas exhibit the highest ET rates. Moving away from agricultural lands toward areas with sparse vegetation leads to a significant decrease in the ET rate. Figure 9 illustrates the reference and daily ET values recorded by lysimeter and calculated by the GeeSEBAL algorithm during satellite overpass days in the Kermanshah study area. The average ET for both methods in 2013 and 2014 stood at 13.61 and 13.95 mm/day for GeeSEBAL and lysimeter, respectively.

In Table 8, the statistical indices for 2013 and 2014 are presented. The correlation coefficients between the measured and estimated ET values using lysimeter and GeeSEBAL are notably high at 0.98 and 0.99, respectively. This suggests a strong alignment of the GeeSEBAL method in determining the ET of wheat. The RMSE values between lysimeter and GeeSEBAL data are 0.42 and 0.55, indicating good agreement. Additionally, NSE and MAE coefficients stand at 0.95, 0.96, 0.40, and 0.42, respectively. With NRMSE values of 0.07 and 0.04 for reference and daily ET, the effectiveness of the GeeSEBAL algorithm in the Kermanshah plain region is well demonstrated. Leveraging
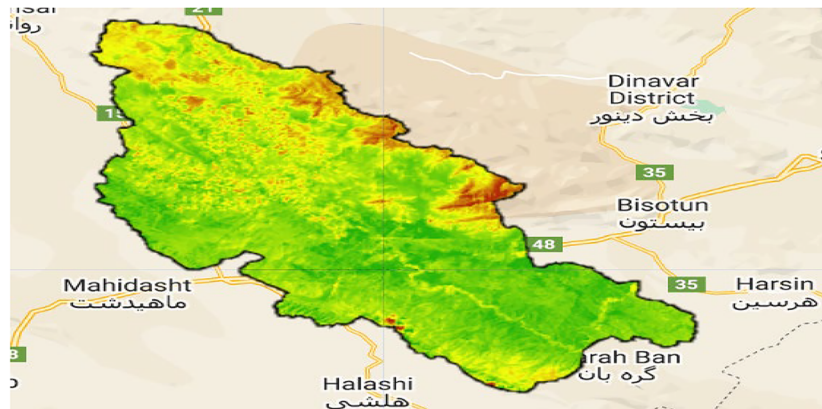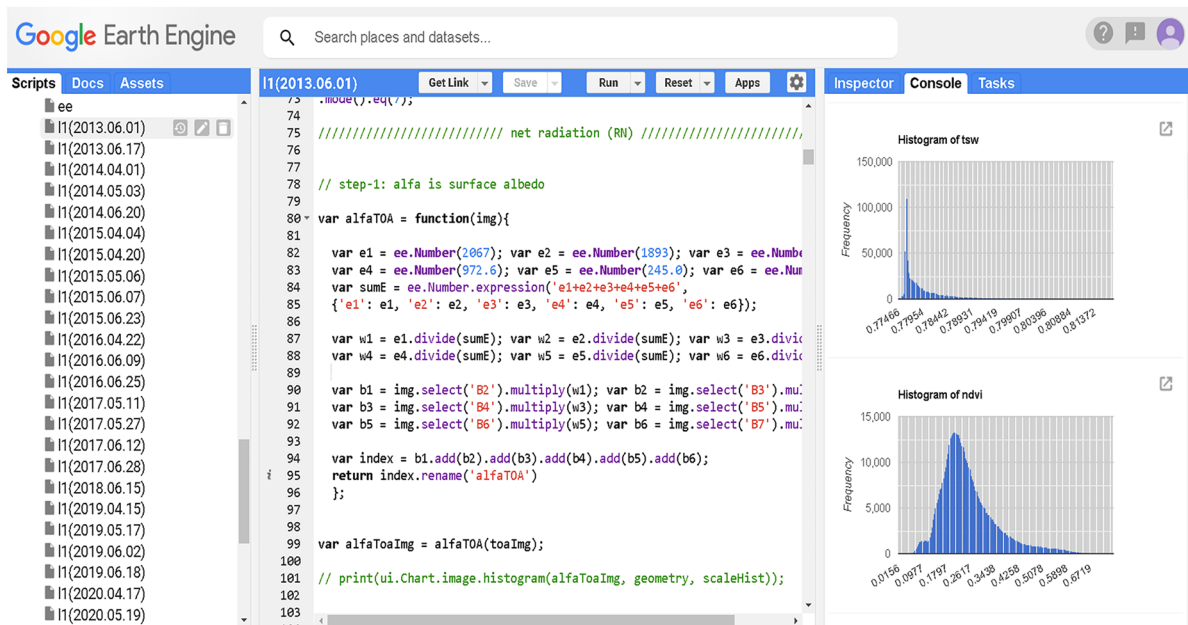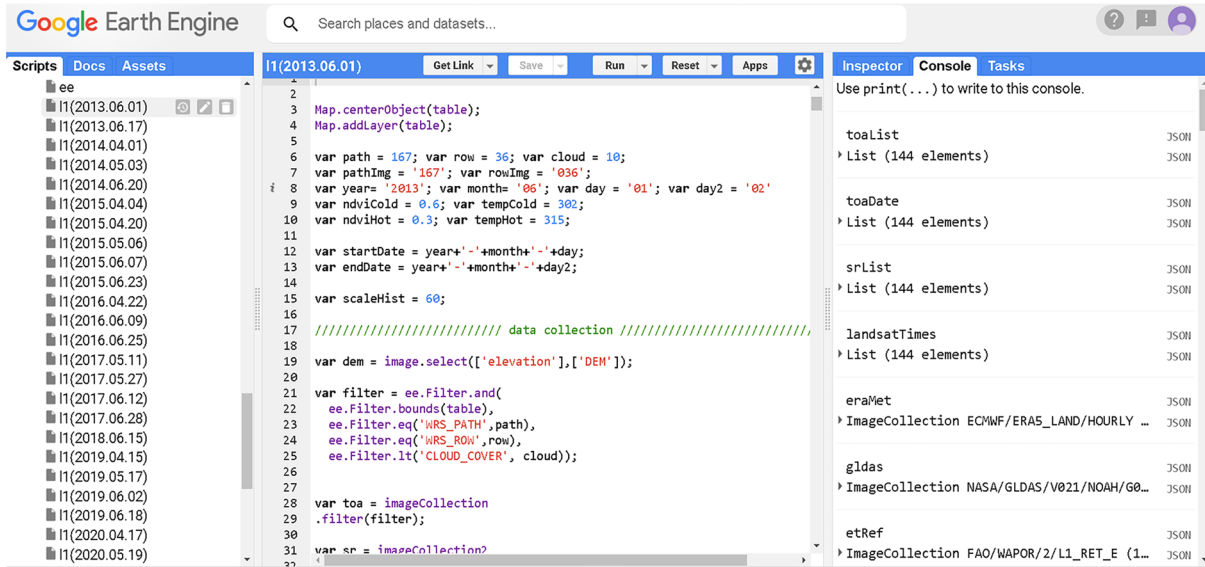
Table 6 Evaluation criteria of indicators

Metric	Equation
R^2	$\dfrac{\left[\sum_{i=1}^{n}(S_i-\overline{S})(O_i-\overline{O})\right]^2}{\left[\sum_{i=1}^{n}(S_i-\overline{S})^2(O_i-\overline{O})^2\right]}$
RMSE	$\left[\dfrac{1}{N}\sum_{i=1}^{N}S_i-O_i\right]^{\frac{1}{2}}$
NRMSE	$\dfrac{RMSE}{\overline{O}}$
NSE	$1-\dfrac{\sum_{i=1}^{N}(O_i-S_i)^2}{\sum_{i=1}^{N}\left(O_i-\overline{O}\right)^2}$
MAE	$\dfrac{\left|\sum_{i=1}^{N}(O_i-S_i)\right|}{N}$

Fig. 5 How to code and extract the ET map in the GEE environment

Table 7 Reference and daily wheat ET values obtained from the GeeSEBAL algorithm for the years 2013 and 2014

Date of image capture	Reference ET GEESE-BAL (mm/day)	Actual ET GEESEBAL (mm/day)	Date of image capture	Reference ET GEESE-BAL (mm/day)	Actual ET GEESEBAL (mm/day)
2013/06/01	6.85	13.78	2018/06/15	6.11	14.44
2013/06/17	8.41	15.94	2019/04/15	4.15	9.65
2014/04/01	2.82	10.03	2019/05/17	5.38	12.75
2014/05/03	5.18	12.93	2019/06/02	6.18	14.06
2014/06/20	7.35	15.37	2019/06/18	6.84	15.56
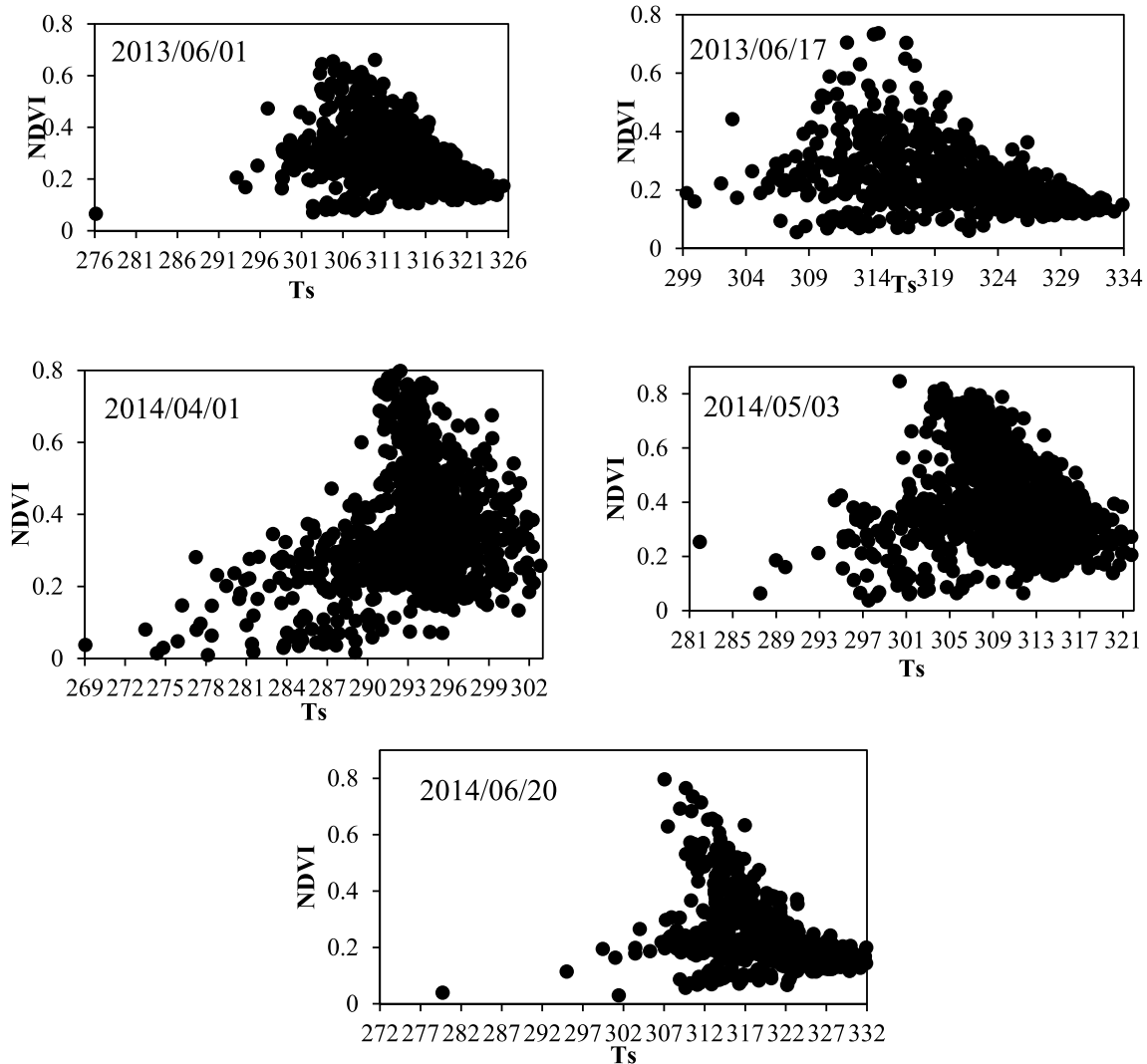
Fig. 6 Trends of NDVI and TS changes calculated in 2013–2014 using the GeeSEBAL model

the benefits of the GEE environment, it is advisable to employ the GeeSEBAL method for estimating wheat plant transpiration and reference ET in this area.

Given that GeeSEBAL effectively fitted the values of wheat ET for the years 2013 and 2014, it is possible to rely on its results for future years as well (Table 9).
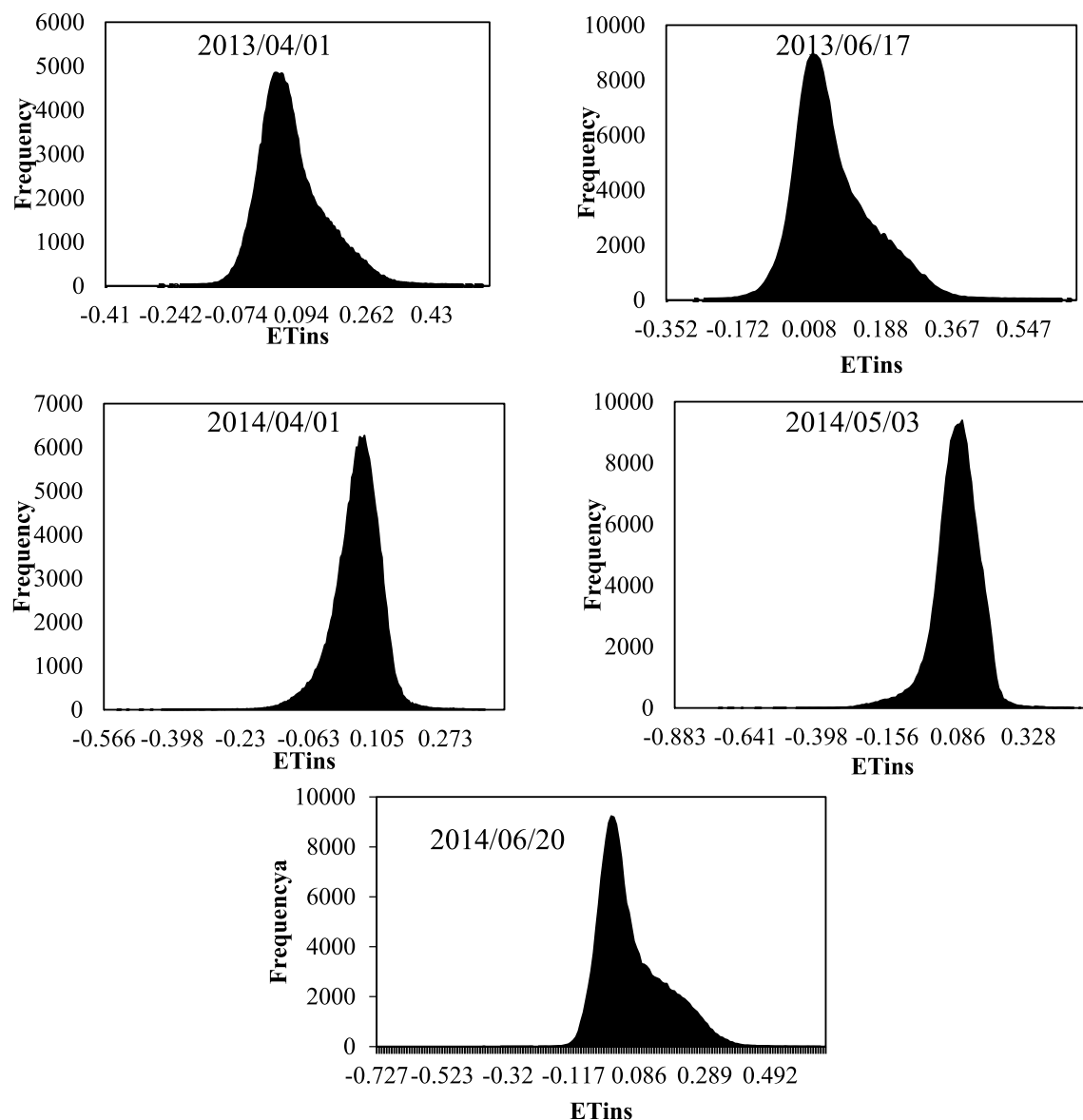
Fig. 7 Instantaneous ET calculated in 2013–2014 using GeeSEBAL model

Changes in ETo are crucial for agricultural water management, irrigation system design, and planning. The linear regression trend shows a consistent increase in daily ET from 2013 to 2022 as depicted in Fig. 10.

Tabari et al. (2011) showed a positive trend in 70% of the stations in western Iran using the Mann–Kendall test and Sen's slope estimator, and in 75% of stations using linear regression for annual ETo series in the region, which is in line with the findings of this study.

Due to the increase in the rate of ET, the maps of actual ET, Trends of NDVI and TS changes, and instantaneous ET have been extracted for the year 2022 in Figs. 11, 12, and 13.

Discussion

Few studies have explored the ET levels using the GeeSEBAL model and Landsat 8 images, making it challenging to contrast the findings of this study with those of other researchers. Santos et al. (2021) introduced the GeeSEBAL code tool, noting its versatility in Earth science applications. Comparisons between EC and estimated data from GeeSEBAL demonstrated the model's effectiveness across various vegetation types and ecosystems, yielding consistently accurate results (RMSD < 0.7 mm/day in most instances). Thus, the tool provides a swift and precise

Fig. 8 Map of actual ET for the wheat growing season in Kermanshah plain.
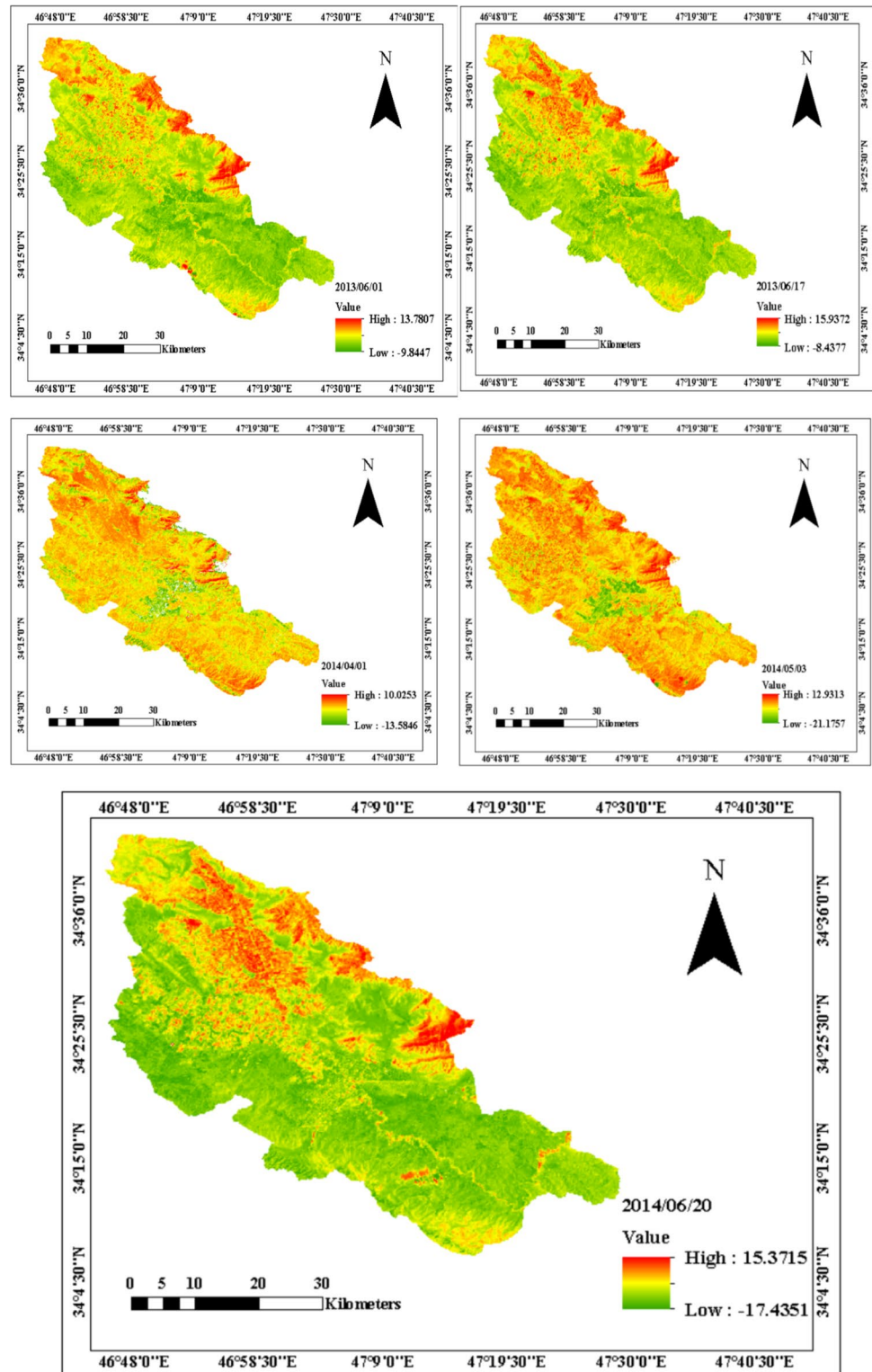
method for estimating ET. In a study by Gonçalves et al. (2022) in a major sugarcane production area, daily ET from GeeSEBAL was compared with EC data, resulting in R^2 and RMSE values of 0.97 and 0.46, respectively. Kayser et al. (2022) utilized Eddy covariance data from

five flow towers in southern Brazil to validate ET estimates. Processing 132 cloud-free Landsat images with adjusted parameters yielded a RMSE of 0.91 and an R^2 of 0.82. Andrade et al. (2024) similarly demonstrated the utility of GeeSEBAL-MODIS for tracking climate change
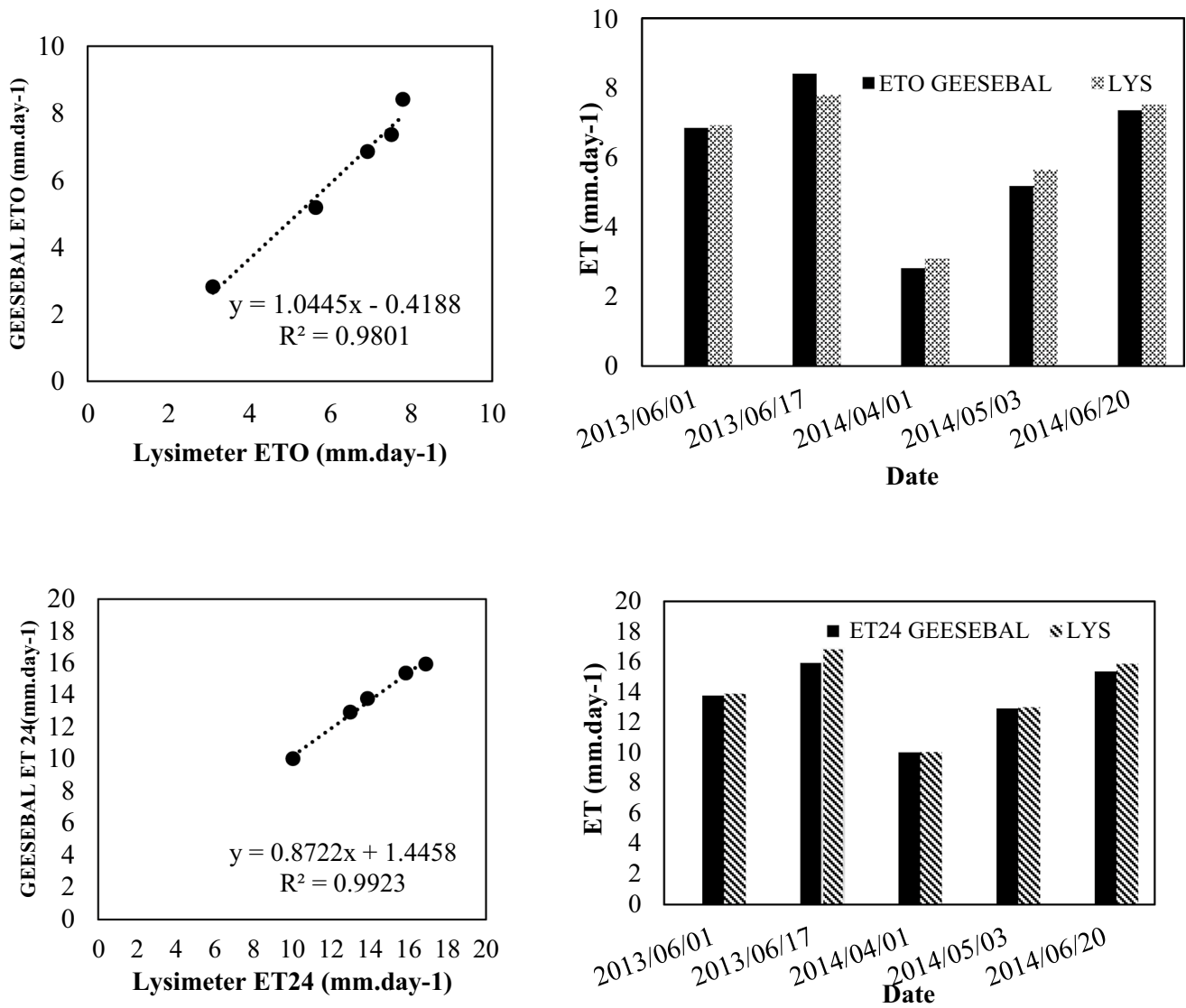
Fig. 9 Reference and daily ET measured by lysimeter and estimated by GeeSEBAL algorithm

Table 8 The performance evaluation results of GeeSEBAL algorithm based on lysimeter data in 2013–2014

Index	Reference ET (mm.day-1)	Actual ET (mm.day-1)
R^2	0.98	0.99
RMSE	0.42	0.55
NRMSE	0.07	0.04
NSE	0.95	0.96
MAE	0.40	0.42

and human-induced effects on ET. This model paves the path for precise global monitoring and enhances progress in worldwide water resource management. In addition,

studies that have compared SEBAL results with lysimeter results for wheat plants will be reviewed. Bala et al. (2016) evaluated and validated ET using SEBAL algorithm and lysimetric data in wheat fields in India. Results from this study revealed that the RMSE of crop-growing period was 0.51 mmd^{-1} for ET_{SEBAL}. NRMSE (0.21) and R^2 (0.91) tests indicated that model prediction is significant, and model can be effectively used for the estimation of ET from SEBAL as input of RS datasets. Rawat et al. (2017) determined wheat ET using the SEBAL model. The results demonstrated that the SEBAL-based ET conformed with lysimeter method with R^2 value of 0.91. Asadi and Kamran (2022) compared the SEBAL, METRIC, and ALARM algorithms for estimating actual ET of wheat in the Parsabad–Moghan region during the years 2016–2019. The

Table 9 Reference and daily wheat ET values obtained from the GeeSEBAL algorithm for the years 2015-2022

Date of image capture	Reference ET GeeSE-BAL (mm/day)	Actual ET GeeSEBAL (mm/day)	Date of image capture	Reference ET GeeSE-BAL (mm/day)	Actual ET GeeSEBAL (mm/day)
2015/04/04	4.03	10.96	2020/04/17	3.83	11.06
2015/04/20	4.84	12.37	2020/05/19	5.82	13.12
2015/05/06	5.63	13.68	2020/06/04	7.24	15.93
2015/06/07	8.04	15.37	2020/06/20	7.45	16.30
2015/06/23	7.90	15.94	2021/04/04	3.54	10.59
2016/04/22	4.47	10.69	2021/06/07	7.61	16.87
2016/06/09	6.69	15.56	2021/06/23	7.69	15.55
2016/06/25	6.98	16.69	2022/04/23	4.99	11.99
2017/05/11	5.42	13.31	2022/05/09	4.87	12.18
2017/05/27	6.76	13.87	2022/06/10	7.64	17.06
2017/06/12	7.20	14.43	2022/06/26	7.98	14.81
2017/06/28	7.51	16.49			

Fig. 10 Daily ET changes of wheat from 2013 to 2022 using GeeSEBAL algorithm
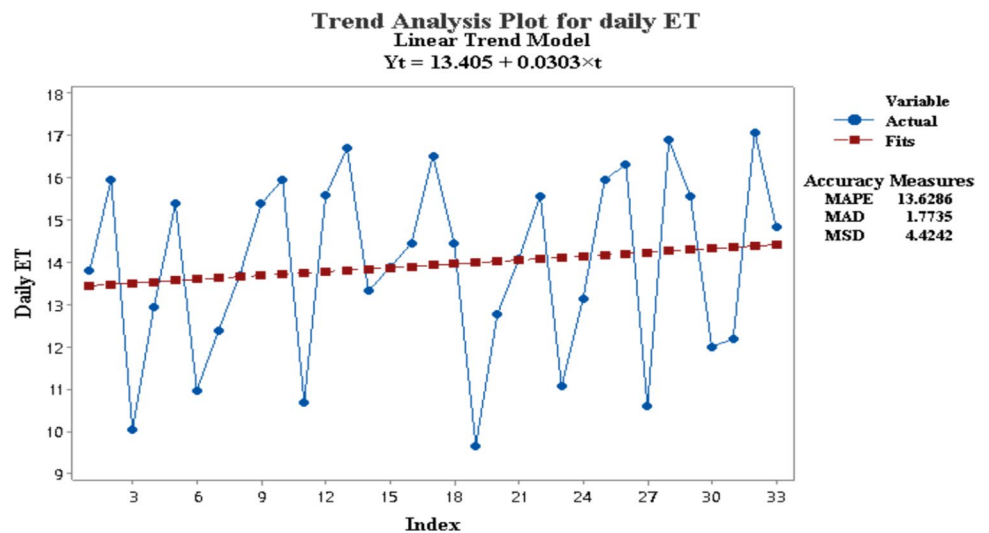
results indicated that the SEBAL algorithm had the lowest RMSE of 0.633 and the highest R^2 of 0.93 compared to the lysimetric results. Zoratipour et al. (2023) estimated the daily ET of wheat using two algorithms (SEBS) and (SEBAL) in the central province of Khuzestan during 2019–2020. According to the results, both SEBAL and SEBS algorithms showed the highest compatibility with lysimeter data ($R^2 = 0.92$ and 0.96, RMSE = 2.15 and 1.53 mm/day, respectively). Given that the exponential coefficient ($R^2 = 0.99$) for determining wheat ET in the GeeSEBAL model has been higher than the results of the SABAL in various studies, it can be concluded that this model is very important for determining ET and can be a suitable replacement for the SABAL algorithm. Also, the

difference of this method from other methods is that it can estimate actual ET for a large area such as a plain without the need for land cover data, while other methods like lysimeters simulate or calculate ET at a point or farm level.

Conclusion

Various algorithms and techniques for calculating ET have been suggested, with remote sensing algorithms and satellite imagery playing an increasingly important role. These methods have consistently demonstrated results, particularly when contrasted with the limitations of using lysimeters for estimating ET (e.g., time consumption, high costs, and
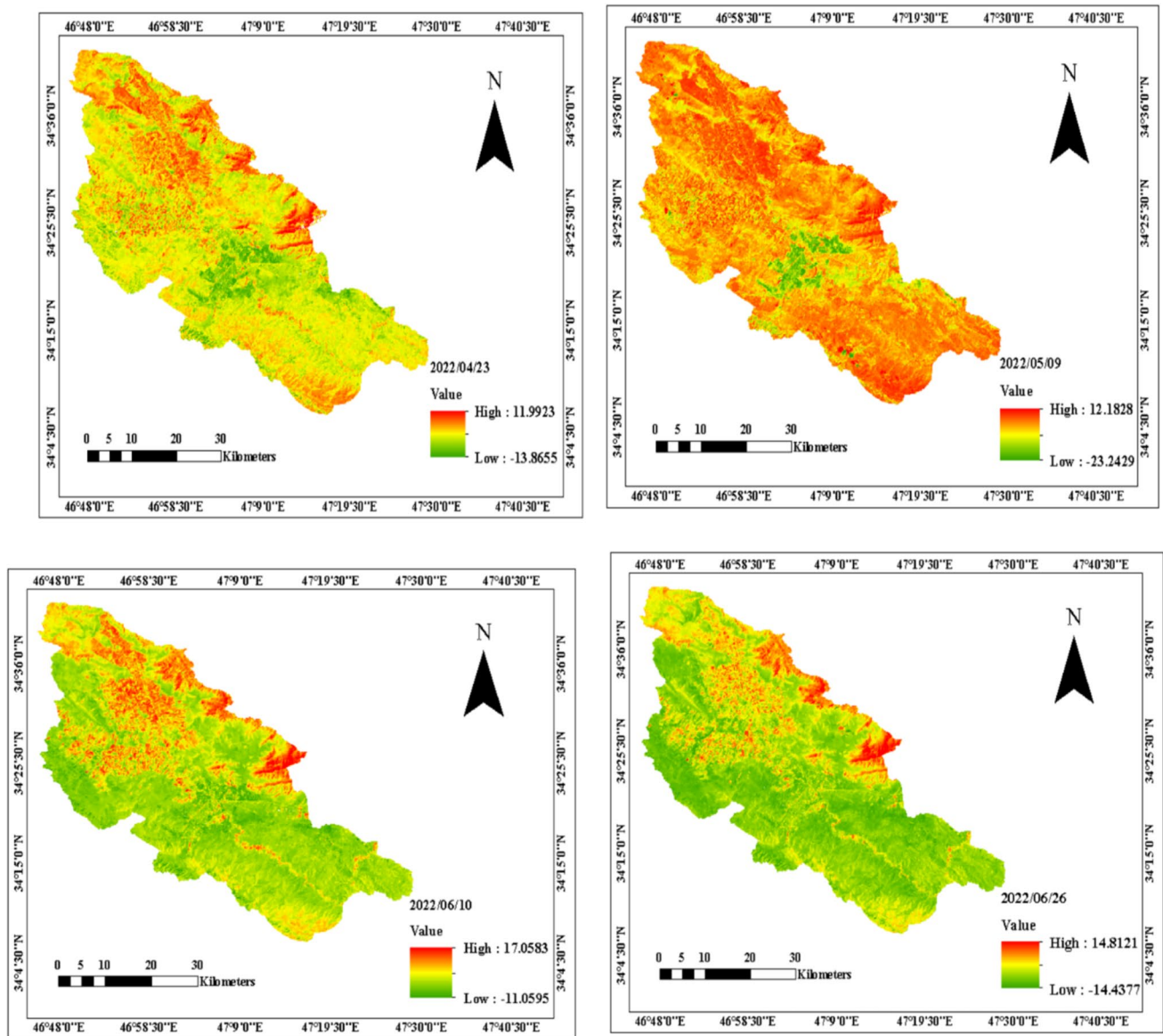
Fig. 11 Maps of actual ET for the wheat growing season for 2022 in Kermanshah plain.

limited data generalization on a large scale). Employing RS approaches, like the GeeSEBAL model, represents a scientific and cost-efficient method for computing ET at a regional level. Recent progress in RS holds promise for estimating actual ET across extensive agricultural regions. This investigation was carried out in the Kermanshah plain utilizing the open-source SEBAL framework and GEE through the API. A comparison of the ET values derived from the GeeSEBAL algorithm and the lysimeter in the study zone uncovers a strong correlation between the results obtained from both techniques. The R^2 values for reference and actual ET were found to be 0.98 and 0.99, respectively. Furthermore,

statistical evaluations employing RMSE, MAE, NSE, and NRMSE metrics revealed a slight quantitative variance in the mean ET data between the two methodologies. Given GeeSEBAL's autonomy from land measurements as inputs, this model possesses worldwide applicability for field and regional inquiries into water and energy balance, as well as water resource management in areas lacking climate data. Ultimately, harnessing global meteorological networks and observational datasets with advanced methods for estimating ET in cloud computing environments, like the OpenET initiative, will bolster agricultural water management on a global scale.
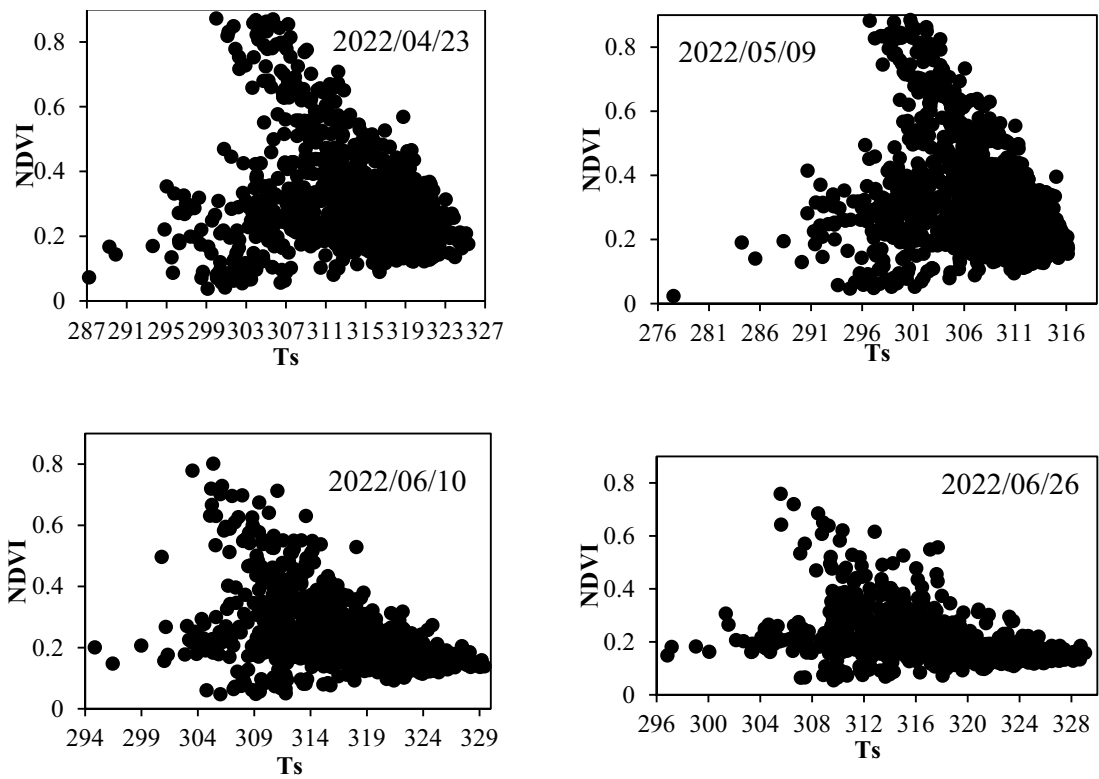
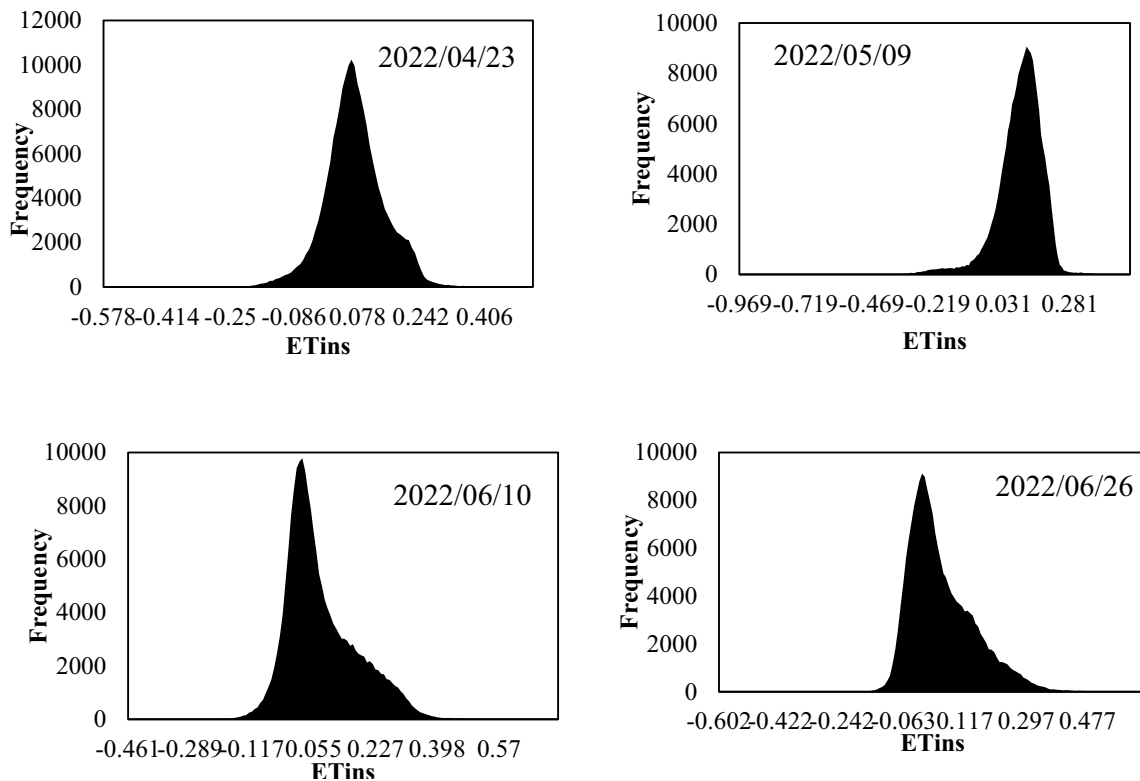**Fig. 12** Trends of NDVI and TS changes calculated in 2022 using the GeeSEBAL model

Fig. 13 Instantaneous ET calculated in 2022 using GeeSEBAL model

Data availability The codes intended to estimate the evaporation and transpiration of the wheat crop were written in the open-source system GEE using the Java programming language.

Declarations

Conflict of interest The authors declare that they have no conflict of interest in this work.

Ethical approval We declare herein that our paper is original and unpublished elsewhere and that this manuscript complies to the Ethical Rules applicable for this journal.

Consent to participate All of the authors consent to participate in this research work.

Consent for publication All of the authors consent to publish this work.

References

Allen RG, Tasumi M, Morse A, Trezza R (2005) A landsat-based energy balance and ET model in Western US water rights regulation and planning. Irrig Drain Syst 19(3):251–268. https://doi.org/10.1007/s10795-005-5187-z

Andrade BC, Laipelt L, Fleischmann A, Huntington J, Morton C, Melton F, Ruhoff A (2024) GeeSEBAL-MODIS: continental-scale evapotranspiration based on the surface energy balance for South America. ISPRS J Photogramm Remote Sens 207:141–163. https://doi.org/10.1016/j.isprsjprs.2023.12.001

Asadi M, Kamran KV (2022) Comparison of SEBAL, METRIC, and ALARM algorithms for estimating actual evapotranspiration of wheat crop. Theoret Appl Climatol 149(1):327–337. https://doi.org/10.1007/s00704-022-04026-3

Bala A, Rawat KS, Misra AK, Srivastava A (2016) Assessment and validation of evapotranspiration using SEBAL algorithm and Lysimeter data of IARI agricultural farm, India. Geocarto Int 31(7):739–764. https://doi.org/10.1080/10106049.2015.1076062

Bastiaanssen WG (2000) SEBAL-based sensible and latent heat fluxes in the irrigated Gediz Basin, Turkey. J Hydrol 229(1–2):87–100. https://doi.org/10.1016/S0022-1694(99)00202-4

Campos I, Neale CM, Arkebauer TJ, Suyker AE, Gonçalves IZ (2018) Water productivity and crop yield: a simplified remote sensing driven operational approach. Agric For Meteorol 249:501–511. https://doi.org/10.1016/j.agrformet.2017.07.018

de Lima CES, de Oliveira Costa VS, Galvíncio JD, da Silva RM, Santos CAG (2021) Assessment of automated evapotranspiration estimates obtained using the GP-SEBAL algorithm for dry forest vegetation (Caatinga) and agricultural areas in the Brazilian semiarid region. Agric Water Manag 250:106863. https://doi.org/10.1016/j.agwat.2021.106863

Ferreira VG, Gong Z, He X, Zhang Y, Andam-Akorful SA (2013) Estimating total discharge in the Yangtze River Basin using satellite-based observations. Remote Sens 5(7):3415–3430. https://doi.org/10.3390/rs5073415

Goncalves IZ, Ruhoff A, Laipelt L, Bispo R, Hernandez FBT, Neale CMU, Marin FR (2022) Remote sensing-based evapotranspiration modeling using GeeSEBAL for sugarcane irrigation management in Brazil. Available at SSRN 4162286. https://doi.org/10.1016/j.agwat.2022.107965

Gorelick N, Hancher M, Dixon M, Ilyushchenko S, Thau D, Moore R (2017) Google earth engine: planetary-scale geospatial analysis for everyone. Remote Sens Environ 202:18–27. https://doi.org/10.1016/j.rse.2017.06.031

Huete AR, Glenn EP (2011) Remote sensing of ecosystem structure and function. Advances in Environmental Remote Sensing. Sensors, Algorithms, and Applications. CRC Press, Boca Raton, pp. 291–320.

Jiang B, Zhang Y, Liang S, Wohlfahrt G, Arain A, Cescatti A, Lund M (2015) Empirical estimation of daytime net radiation from shortwave radiation and ancillary information. Agric For Meteorol 211:23–36. https://doi.org/10.1016/j.agrformet.2015.05.003

Karandish F, Hoekstra AY (2017) Informing national food and water security policy through water footprint assessment: the case of Iran. Water 9(11):831

Kayser RH, Ruhoff A, Laipelt L, de Mello Kich E, Roberti DR, de Arruda Souza V, Neale CMU (2022) Assessing geeSEBAL automated calibration and meteorological reanalysis uncertainties to estimate evapotranspiration in subtropical humid climates. Agric For Meteorol 314:108775. https://doi.org/10.1016/j.agrformet.2021.108775

Li MF, Tang XP, Wu W, Liu HB (2013) General models for estimating daily global solar radiation for different solar radiation zones in mainland China. Energy Convers Manag 70:139–148. https://doi.org/10.1016/j.enconman.2013.03.004

Munoz-Sabater J, Dutra E, Agustí-Panareda A, Albergel C, Arduini G, Balsamo G, Boussetta S, Choulga M, Harrigan S, Hersbach H, Martens B, Miralles DG, Piles M, Rodríguez-Fernandez NJ, Zsoter E, Buontempo C, Thépau JN (2021) ERA5- Land: a state-of-the-art global reanalysis dataset for land applications. Earth Syst Sci Data Discuss 2021:1–50. https://doi.org/10.5194/essd-13-4349

Nazari B, Liaghat A, Parsinejad M (2013) Development and analysis of irrigation efficiency and water productivity indices relationships in Sprinkler Irrigation Systems. Int J Agron Plant Prod 4(3):515–523

Oliveira LM, Montenegro SM, Silva BBD, Antonino AC, de Moura AE (2014) Evapotranspiração real em bacia hidrográfica do Nordeste brasileiro por meio do SEBAL e produtos MODIS. Revista Brasileira De Engenharia Agrícola e Ambiental 18:1039–1046

Patel NN, Angiuli E, Gamba P, Gaughan A, Lisini G, Stevens FR, Trianni G (2015) Multitemporal settlement and population mapping from Landsat using Google earth engine. Int J Appl Earth Obs Geoinf 35:199–208. https://doi.org/10.1016/j.jag.2014.09.005

Rawat KS, Bala A, Singh SK, Pal RK (2017) Quantification of wheat crop evapotranspiration and mapping: a case study from Bhiwani District of Haryana, India. Agric Water Manag 187:200–209. https://doi.org/10.1016/j.agwat.2017.03.015

Richter R, Kellenberger T, Kaufmann H (2009) Comparison of topographic correction methods. Remote Sens 1(3):184–196. https://doi.org/10.3390/rs1030184

Santos LLD, Fleischmann AS, Kayser RHB, Ruhoff AL (2021) GeeSEBAL: um aplicativo para estimativas de séries temporais de evapotranspiração em alta resolução espacial. Simpósio Brasileiro de Recursos Hídricos. Porto Alegre: ABRHidro.

Silva BB, Mercante E, Boas MAV, Wrublack SC, Oldoni LV (2018) Satellite-based ET estimation using Landsat 8 images and SEBAL model. Revista Ciência Agronômica 49(2):221–227. https://doi.org/10.5935/1806-6690.20180025

Sun Z, Wei B, Su W, Shen W, Wang C, You D, Liu Z (2011) Evapotranspiration estimation based on the SEBAL model in the Nansi Lake Wetland of China. Math Comput Model 54(3–4):1086–1092. https://doi.org/10.1016/j.mcm.2010.11.039

Sun H, Chen L, Yang Y, Lu M, Qin H, Zhao B, Yan D (2022) Assessing variations in water use efficiency and linkages with land-use changes using three different data sources: a case study of the Yellow river, China. Remote Sens 14(5):1065. https://doi.org/10.3390/rs14051065

Tabari H, Marofi S, Aeini A, Hosseinzadeh Talaee P, Mohammadi K (2011) Trend analysis of reference evapotranspiration in the western half of Iran. Agric For Meteorol 151(2):128–136. https://doi.org/10.1016/j.agrformet.2010.09.009

Venancio LP (2019) Remote sensing approaches for evapotranspiration and yield estimations on irrigated corn fields⸝

Volk JM, Huntington JL, Melton F, Minor B, Wang T, Anapalli S, Anderson M (2023) Post-processed data and graphical tools for a CONUS-wide eddy flux evapotranspiration dataset. Data Brief 48:109274. https://doi.org/10.1016/j.dib.2023.109274

Wang Y, Zhang S, Chang X (2020) Evapotranspiration estimation based on remote sensing and the SEBAL model in the Bosten Lake basin of China. Sustainability 12(18):7293. https://doi.org/10.3390/su12187293

Wu S, Ben P, Chen D, Chen J, Tong G, Yuan Y, Xu B (2018) Virtual land, water, and carbon flow in the inter-province trade of staple crops in China. Resour Conserv Recycl 136:179–186. https://doi.org/10.1016/j.resconrec.2018.02.029

Xiong J, Thenkabail PS, Gumma MK, Teluguntla P, Poehnelt J, Congalton RG, Thau D (2017) Automated cropland mapping of continental Africa using Google Earth Engine cloud computing. ISPRS J Photogramm Remote Sens 126:225–244. https://doi.org/10.1016/j.isprsjprs.2017.01.019

Yao F, Wang J, Wang C, Crétaux JF (2019) Constructing long-term high-frequency time series of global lake and reservoir areas using Landsat imagery. Remote Sens Environ 232:111210. https://doi.org/10.1016/j.rse.2019.111210

Zhou X, Bi S, Yang Y, Tian F, Ren D (2014) Comparison of ET estimations by the three-temperature model, SEBAL model and eddy covariance observations. J Hydrol 519:769–776. https://doi.org/10.1016/j.jhydrol.2014.08.004

Zoratipour E, Mohammadi AS, Zoratipour A (2023) Evaluation of SEBS and SEBAL algorithms for estimating wheat evapotranspiration (case study: central areas of Khuzestan province). Appl Water Sci 13(6):137. https://doi.org/10.1007/s13201-023-01941-2